A Gigaseal Obtained with a Self-Assembled Long-Lifetime Lipid Bilayer on a Single Polyelectrolyte Multilayer-Filled Nanopore

Kaori Sugihara, János Vörös, and Tomaso Zambelli*

Laboratory of Biosensors and Bioelectronics, Institute for Biomedical Engineering, ETH Zurich, Gloriastrasse 35, CH-8092 Zurich, Switzerland

ABSTRACT A lipid bilayer with gigaohm resistance was fabricated over a single 800 nm pore in a Si_3N_4 chip using 50 nm liposomes. The nanopore was prefilled with a polyelectrolyte multilayer (PEM) that triggered the spontaneous fusion of the lipid vesicles. Pore-forming peptide melittin was incorporated in the bilayer, and single channel activities were monitored for a period of 2.5 weeks. The long lifetime of the system enabled the observation of the time-dependent stabilization effect of the melittin open state upon bias application.

After the invention of the patch clamp, different methodologies for the fabrication of *in vitro* membrane systems have been proposed for the application of drug screening as well as for the investigation of membrane peptides and proteins. Black lipid membranes (BLMs),[1,2] where an artificial lipid membrane is spanned over a micropore by painting lipid molecules dissolved in organic solvents, have become a model system for monitoring single channel events of pore-forming peptides[3,4] and ion channels.[5] Nevertheless, the system remains low throughput because of its delicate preparation procedure and short lifetime. Additionally, the organic solvent residuals remaining in the lipid membrane disrupt some channels, limiting the applications. Supported lipid membranes (SLMs),[6−11] where a lipid bilayer is directly created on a flat electrode by fusing liposomes, are an alternative because the liposome fusion is a self-assembling and reproducible fabrication method, while the solid support prolongs the membrane lifetime, all of which potentially make the system high throughput. However, the system suffers from low sensitivity mainly because the small distance between the electrode and the lipid bilayer causes ion accumulation that stops the current across the channels. The obvious and challenging solution for the dilemma between BLM and SLM is the fabrication of a lipid bilayer in the freestanding configuration by liposome fusion. Recently, Schmitt *et al.* have chemically modified the surface of porous alumina to promote the fusion of large unilamellar vesicles (LUVs) directly on the nanopore array obtaining a free-standing lipid bilayer.[12] Nanopores are also known to enhance the robustness and the lifetime of the lipid bilayer as reported in several other works.[13,14] However, the anodized alumina produces too many pores (~100 000), resulting in a serious current leakage from uncovered pores, preventing the monitoring of single channel events. Standard semiconductor lithography allows for a straightforward control over the pore density and the aspect ratio of nanopore arrays,[13,14] yet there is no established procedure to fuse vesicles on such pore arrays, except for a non-self-assembling approach.[15] In addition, the fabrication of nanopores smaller than 100 nm demands electron beam lithography, which leads back to the low fabrication throughput and high cost.

On the other hand, polymers have been widely exploited in both BLMs[16] and SLMs[17−20] to stabilize bilayers or as a cushion between bilayers and surfaces. Several groups have demonstrated a polymer-sandwiched lipid bilayer and detected single ion channel transports, showing that the polymer enhances the lifetime of the lipid bilayer while remaining transparent for ions.[16,21,22] Nevertheless, those fabrication methods (painting or folding) are non-self-assembling, therefore hindering high-throughput applications. Polyelectrolyte multilayers (PEMs),[23−26] besides other films
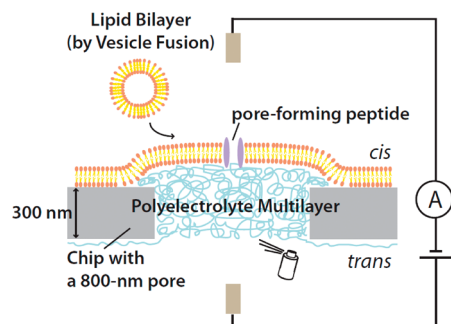
Figure 1. Schematic of the device. The chip consists of a 300 nm Si/Si$_3$N$_4$ membrane and a single 800 nm pore produced by standard photolithography (see ref 13 for a detailed description). A polyelectrolyte multilayer (PEM) is sprayed from the *trans* side to close the pore. Small unilamellar vesicles (SUVs) are simply added from the *cis* side to spontaneously form a lipid bilayer.

such as noncharged polymers[27] and lipidic films,[28] have been found to trigger the fusion of oppositely charged lipid vesicles into a planar lipid bilayer,[20,29−32] providing an interesting alternative to create self-assembling polymer-supported bilayers; however, the electrical property of the lipid bilayer has been reported as leaky.[30]

In this work, we report a unique fabrication strategy of a giga-sealing lipid bilayer over a single 800 nm pore in a Si/Si$_3$N$_4$ chip by prefilling the pore with a PEM to enable the spontaneous fusion of 50 nm liposomes over the pore (Figure 1). The prefilled PEM functions, on one hand, as a "surface", promoting liposome fusion as well as enhancing the lifetime of the obtained bilayer, while it remains transparent for ions, maintaining a pore-spanning configuration. Our approach needs only a single submicrometer pore fabricated by standard photolithography and 50 nm small unilamellar vesicles (SUVs) obtained by the common extrusion procedure, freeing us from pursuing the labor-intensive fabrication of "smaller pores and larger vesicles" required for the direct fusion on nanopores. To test the feasibility of the obtained gigaseal for monitoring the peptide channel activities and the lifetime of the functioning lipid bilayer, melittin, which is known as a voltage-gated channel, was incorporated directly from the solution and single channel events were monitored.

RESULTS AND DISCUSSION

The sample fabrication process is illustrated in the schematic in Figure 1. The pore with 800 nm diameter in a 300 nm Si/Si$_3$N$_4$ membrane is designed to be small enough to avoid the leakage current but large enough to maintain the low aspect ratio (0.375). The PEM is sprayed[33,34] from one side of the chip while the lipid bilayer is formed from the other side (back-spraying method). When the PEM film and the lipid bilayer were deposited on the same side, the PEM cushion between the Si$_3$N$_4$ membrane and the lipid bilayer induced a leakage current, preventing the establishment of a gigaseal.
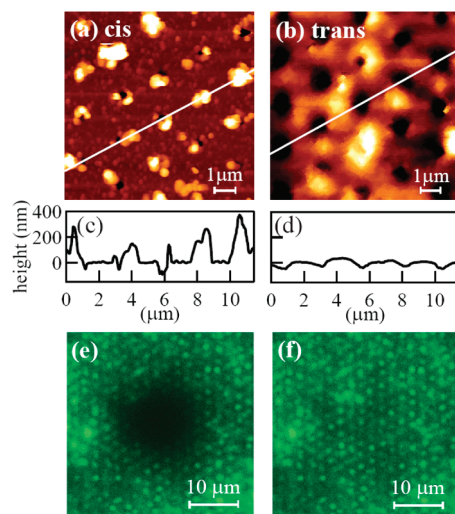

Figure 2. Characterization of the PEM film and the lipid bilayer. (a,b) Topographical AFM images after the deposition of PEM and (c,d) corresponding cross sections along the highlighted line, taken from the *cis* and *trans* side, respectively. The thickness of the PEM film in the nonpore area on the *trans* side was determined as 100 nm by the scratching method at the edge of the chip. (e,f) Fluorescent recovery after photobleaching (FRAP) measurements by confocal laser scanning microscope (CLSM) taken from the *trans* side (e) just after the bleaching and (f) after 30 min. The full recovery confirms the lipid bilayer formation. Note that the focus was adjusted on the *cis* side. The small dots correspond to the pore array.

First, after spraying one polyethyleneimine (PEI) layer as an anchoring layer, a (PSS/PAH)$_{24}$ film, which is a well-known polymer couple frequently used to fabricate a smooth film,[35,36] was sprayed onto the *trans* side of the chip, and a PEI layer was subsequently sprayed from the *cis* side. Both the last PAH layer on the *trans* side and the PEI layer on the *cis* side are meant to give the PEM a net-positive charge, which is important for the following vesicle fusion. As positively charged polyelectrolyte, such as PAH and PLL, has been known to trigger the vesicle fusion,[37] we found that the PEI top layer functions in a similar way. To characterize the PEM deposition, topographical images of the chip after PEM deposition were taken by atomic force microscopy (AFM) from the *cis* side (Figure 2a,c) and the *trans* side (Figure 2b,d). For imaging, chips with pore arrays were used in order to localize the pores easier. A pattern of bumps with a few hundred nanometers height were observed on the *cis* side: by comparison with AFM images of the bare chip before PEM deposition, we can infer that the bumps are due to the PEM film. Although the filling of the pore is not uniform in each pore, we can conclude that all of the pores are closed by PEM since even the deepest point in the PEM-filled pores is less than 80 nm, while AFM scanning is impractical over 800 nm pores without the PEM film because of the lack of the force feedback over the empty pores. The AFM image of the *trans* side (Figure 2b) shows a pattern of hollows with less than a hundred nanometers in correspondence to the pore pattern. From these in-

vestigations, the shape of the PEM film can be schematically modeled as Figure 1. Such a complete nanopore clogging by PEM films has been reported extensively.[38−41] The growth mechanism of the same PEM film as we used (PSS/PAH) in nanopores with diameters of 200−500 nm has been studied in detail by Roy and co-workers with transmission electron microscope and gas-flow porometry,[42] where they have observed two different PEM growth kinetics, which they linked to the diffusion of the polyelectrolytes in the pores.

In order to form a lipid bilayer over the PEM-filled pores, a solution containing negatively charged SUVs (DOPS, ϕ = 50 nm, 3 mg/mL) was simply added from the *cis* side and incubated for 20−30 min at 55 °C followed by a rinse, where both the electrical attraction and the high temperature were exploited to promote vesicle rupture.[37] Although the bilayer formation was also observed at lower temperatures occasionally, the elevated temperature increases the success rate. The formation of the lipid bilayer and its mobility were proven by fluorescent recovery after photobleaching (FRAP) using a confocal laser scanning microscope (CLSM) imaging from the *trans* side (Figure 2e,f). The bleached circular zone was fully recovered within 30 min, proving the fluidity of lipid molecules throughout the pores. When we added the vesicle solution without the PEM deposition, the fluorescent intensity in the pores was much lower than over the nonpore area, indicating the lack of lipid molecules over the empty pores. From the time evolution of the fluorescent intensity in the bleached zone, we derived a diffusion coefficient D of $(0.08 \pm 0.04) \times 10^{-8}$ cm^2 s^{-1} (according to the equation provided in ref 43), which is comparable to the value for the lipid bilayer on a PEM film reported previously ($0.021−0.072 \times 10^{-8}$ cm^2 s^{-1}), where the 1 or 2 orders of magnitude smaller value of D compared to that on a glass slide has been linked either to the strong coupling between the lipid molecules and the oppositely charged PEM or to the result of insufficient connectivity of the lipid bilayer.[20,30,37]

The electrical resistance of the lipid bilayer was estimated by electrochemical impedance spectroscopy (EIS) using a chip with a single pore (CSP) and two Ag/AgCl electrodes (Figure 3). At low frequency (red dotted circles in Figure 3), where the impedance Z is mainly dominated by the resistance R, the impedance Z of CSP and CSP + PEM are $Z \sim R \sim$ 1.5 and 19 MΩ, respectively, while it increases up to 1 GΩ after the deposition of the lipid bilayer, indicating the formation of a gigaseal (see Supporting Information for a detailed discussion). The drastic increase of the resistance after the vesicle fusion was observed at every attempt: a gigaseal was established with a 30% success rate, while a resistance between 500 and 800 MΩ was measured the rest of the time. Although gigaseal was obtained, resistivity calculated from the pore area is 5 Ωcm^2, which
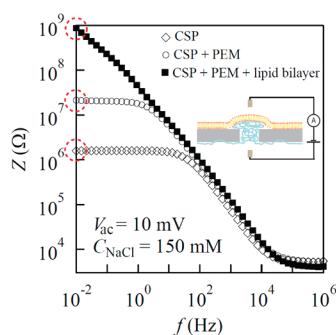

Figure 3. Electrical resistance of the lipid bilayer. Electrochemical impedance spectroscopy (EIS) measurement of a chip with a single pore (CSP, ◇), of CSP covered with PEM (CSP + PEM, ○), and of CSP + PEM with a lipid bilayer (CSP + PEM + lipid bilayer, ■). The drastic increase of the impedance at low frequency at $f = 10^{-2}$ Hz up to 1 GΩ after the deposition of a lipid bilayer indicates the formation of the gigaseal.

is 6 orders of magnitude lower than that in BLM.[1] In general, PEM-supported lipid bilayers are known to have a poor electrical resistivity,[30] as a result of defects in the bilayer. In addition, in our system, the imperfect sealing between the chip and the lipid bilayer at the edge of the pore as well as the electrostatic interaction between the positively charged PEM and the negatively charged lipids might have also influenced the transport properties, leading to the low resistivity. Nevertheless, the change in the resistance by 2 orders of magnitude between before and after the lipid bilayer deposition tells us that the total defect area is 1% of the pore area, hypothesizing that the obtained lipid bilayer is made of a perfect insulator membrane with defects. Our data show that the gigaseal is achievable with such a PEM lipid bilayer composite by exploiting the 800 nm pore. Here, we note that we used a thin PEM film, and both fabrication and the experiment were conducted with buffer solution with monovalent ions at high concentration in order to make the PEM as ion permeable as possible since PEMs are known to act as ion-selective membranes especially for divalent ions and at low salt concentration.[44] As we expected, the data prove that the resistance of the PEM is low enough not to disturb the monitoring of the peptide channel activities because both the resistance of CSP (1.5 MΩ) and CSP + PEM (19 MΩ) are orders of magnitudes lower than that with lipid bilayer (1 GΩ).

Next, to test that the obtained sealing is sufficient to observe peptide channel activities, we performed experiments with a pore-forming peptide: melittin. Melittin is the main active component of bee venom that has attracted interest because of its antimicrobial activity (*e.g.*, against *Borrelia burgdorferi* bacteria, which causes lyme disease,[45] yeast *Candida albicans*,[46] *Mycoplasma hominis*, and *Chlamydia trahomatis*[47]) and also has been exploited as a model peptide for studying the lipid−peptide interactions.[48] It is a bar-type peptide, which adsorbs on lipid bilayers with various orienta-
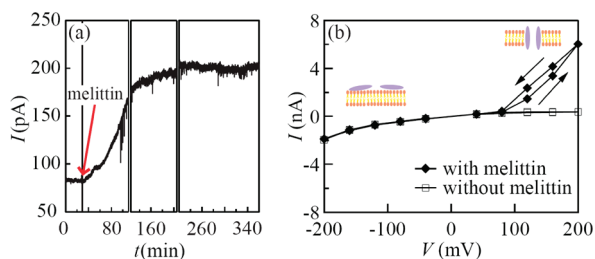
Figure 4. Melittin incorporation. (a) Time evolution of the current at $V = 60$ mV upon melittin addition to the *cis* side ($C_{melittin} = 166$ μg/mL, $C_{NaCl} = 0.5$ M). The red arrow indicates the moment when the melittin solution was injected into the device. (b) Voltage-gated characteristics of melittin. $I-V$ curves were measured with (♦) and without (□) melittin. The two typical responses of incorporated melittin, *i.e.*, the asymmetrical $I-V$ curve and the current hysteresis were both observed after the addition.
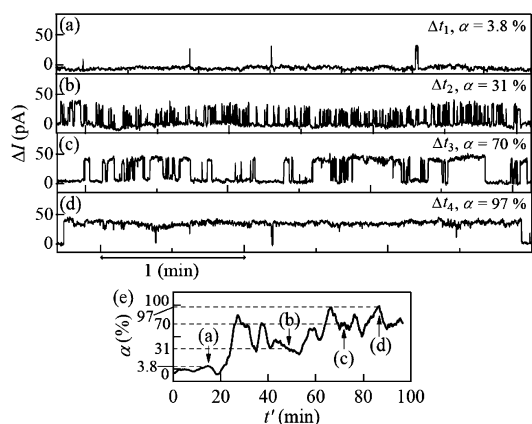

Figure 5. Monitoring of single channel events. Single channel activities were recorded at $V = 100$ mV. The current changes with respect to the baseline ΔI were monitored continuously over 100 min after the bias application. Δt_1 corresponds to 15 min $< t <$ 18 min 20 s (a), Δt_2 to 48 min 48 s $< t <$ 52 min 8 s (b), Δt_3 to 71 min 48 s $< t <$ 75 min 8 s (c), and Δt_4 to 86 min 42 s $< t <$ 90 min 2 s (d). (e) Plot of the channel-opening rate α during $t' < t < (t' + 200)$ *versus* t'. The four arrows indicate the a−d situations.

tions such as surface, transmembrane, and pseudotransmembrane orientations, while it forms a channel as an oligomer upon applying a certain potential (to avoid the confusion between "pores" in Si_3N_4 membrane and in the bilayer, we will use the word "channel" for peptide pores). We chose this peptide because identification of the channel activity is straightforward thanks to its voltage-gated properties as extensively reported in literature.[4,49] Melittin incorporation was characterized by monitoring the change in the current I across the lipid bilayer before and after the addition of melittin in the *cis* side. Figure 4a shows the change in the current I as a function of time at a constant voltage $V = 60$ mV, whereby a positive voltage corresponds to the situation where higher voltage is applied to the *cis* side relative to the *trans* side. We note that a higher salt concentration of 0.5 M NaCl was used in this and the rest of the experiments in order to increase the solution conductivity for the efficient observation of the channel activity.[4,49−52] Although the change of the salt concentration has been known to affect the structure of the PEM film,[53−55] the lipid bilayer remained intact as confirmed by the remaining high electrical resistance. A current increase was observed after the addition of melittin (see the arrow in Figure 4a) until it saturated at $I \sim 200$ pA in 200 min, confirming that the lipid bilayer became porous due to the presence of melittin. The current increase is continuous, while stepwise current increase has been reported in ring-type peptide channels such as gramicidin.[3] The mechanism of the channel formation in melittin is different from those ring types due to its bar shape: It is known to be more like formation of a defect, where the high-energy edge of the lipid bilayer is subsequently covered by several monomers.[48] The insertion mechanism, the fluctuation of channels as an ensemble, contribution of channels outside of the pore as well as lack in the time resolution may explain the nonstep increase (see also the comment[56]). As a further step to verify the melittin functionality, we investigated its voltage-gated characteristics. It is known that when melittin is added only from

one side of the bilayer, it forms channels with higher probability if a higher voltage is applied on the melittin-added side because of the unbalanced molecular charge distribution of melittin.[4,49] Figure 4b shows $I-V$ curves before and after the addition of melittin from the *cis* side. With melittin, a major nonlinear current increase occurs only in the positive bias larger than 80 mV, indicating channel opening, while it is not observed without melittin. Both polarity of the voltage associated with the melittin-added side and the threshold voltage are in a good agreement with previous works.[4,49] Additionally, a current hysteresis that has also been reported and interpreted as melittin channels maintaining their open state for a while after reversing the potential sweep[4,57] is seen. The results confirm that the widely known voltage-gated characteristic of melittin is well reproduced in our system. Here we note that a few orders of magnitude higher concentration of melittin was required to observe the asymmetrical $I-V$ curve compared to other works[4,49,57] because our total pore area is several orders of magnitude smaller than that of the referred works. Even at the high concentration, melittin did not break the lipid bilayer as reported since negatively charged lipids strongly suppress the lysis induced by melittin even at a high concentration of 100 μg/mL,[58,59] while in systems with electrically neutral lipids, addition of melittin breaks the BLM[4] or induces pores without applying any voltages even at a few μg/mL.[58,59] The concentration of melittin is so high that tetramers may have been formed in the solution,[60] which contribute to the pore formation to a lesser extent than monomers.

Finally, single channel activities were recorded upon optimization of melittin concentration ($C_{melittin} = 33$ μg/mL) and of the applied bias voltage ($V = 100$ mV). Figure 5 shows the time evolution of the current at differ-

ent time points since the bias was applied. The current jumps between two discrete states separated by 40 pA (determined by the histogram over the whole experiment), as shown in Figure 5a–d, are interpreted as single channel activity with a channel conductance of g_s = 400 pS, as very similar current fluctuations for single melittin channel events have been extensively reported.[4,49−52] The fact that the similar single channel activities to conventional BLM system was observed implies that the difference in the condition of our system from BLMs (e.g., the presence of the PEM film or the electrostatic interaction between the PEM and the lipids) did not affect the melittin activities significantly. Such events could be monitored continuously for a couple of hours repeatedly over 2.5 weeks (data after 1 and 2 weeks are provided in Supporting Information) until a sudden decrease of the membrane resistance, which indicates the breakdown of the membrane. This is one of the longest functioning lipid bilayer lifetimes,[21] which is attributed to the robustness conferred by the PEM film. In the previous reports, a variety of channel conductance have been observed[4,49−52] (e.g., 500 pS at $C_{melittin}$ = 2 μg/mL with a POPC system in 5 M NaCl,[51] 7−10 pS at $C_{melittin}$ = 3 ng/mL with an asolectin lipid bilayer in 1 M NaCl[50]), and also channel size has been studied by nonelectrical methods,[61−63] which are known to strongly depend on the melittin concentration, $C_{melittin}$.[62] In our work, a few orders of magnitude higher $C_{melittin}$ than those works was used as described previously. Thus, although the conductance is high, the result is compatible to the other works.

In Figure 5a–d, four different channel-opening behaviors were recorded. The open state (ΔI = 40 pA) was more frequently observed as time elapses. To quantitatively analyze this chronological channel behavior, we defined a channel-opening rate α over 200 s: α = (total channel-opening time Δt_{open})/200 s. The channel-opening rate α was calculated at given time t' with the time interval of next 200 s ($t' < t < t' + 200$ s) and

plotted against t' in Figure 5e. Although not monotonous, an increasing tendency of the channel-opening rate was observed as time elapses, which implies the stabilization of the open state of the channel by applying the voltage. Pawlak et al. mentioned a similar effect in ref 4. A recent paper has revealed that the adsorption of melittin induces a mechanical stress, making the lipid bilayer thinner, which they have related to the channel formation.[64] We assume the long-time mechanical stress imposed by the cross-membrane voltage due to electrical attraction of the opposite charge accumulated on the surface of the lipid bilayer may explain the observed time-dependent stabilization of the channels in a similar way.

CONCLUSIONS

We developed a giga-sealing lipid bilayer by spontaneous vesicle fusion on a PEM-filled nanopore. The novelty of our concept was to prefill the pore with PEM resulting in a double advantage:

(i) It enabled us to form a lipid bilayer from SUVs (self-assembling and organic solvent free method), where we underline the versatility of our method to be able to use small vesicles obtained by common extrusion together with a submicrometer pore fabricated by standard photolithography, both of which are high-throughput fabrication methods.

(ii) The PEM confers a strong mechanical robustness to the system. The lifetime of the functioning lipid bilayer was shown with the single peptide channel events monitored over 2.5 weeks. The long lifetime of the system allowed us to observe the increase in the channel-opening rate depending on the duration of the bias application, indicating a channel stabilization mechanism.

As an application, ion channels that do not go into lipid membranes spontaneously can be incorporated to the system by proteoliposome fusion or using cell fragments for ion-channel sensors.

MATERIALS AND METHODS

Si/Si$_3$N$_4$ Chips: The chips were fabricated by Leister (CH) according to the procedure described in ref 65. The Si$_3$N$_4$ membrane is 300 nm thick either with a single pore or with a pore array. In both cases, pores have the diameter of 800 nm (separated by a distance of 2 μm for the pore array).[13,49] The chips were preliminarily cleaned for 15 min by an oxygen plasma cleaner (PDC-32G, Harrick, USA) just before the experiments.

Buffer Solution (HEPES-2): The buffer solution was prepared with 10 mM 4-(2-hydroxyethyl)piperazine-1-ethanesulfonic acid (HEPES) purchased from Fluka (Buchs, Switzerland) and either at 0.15 or 0.5 M sodium chloride (Fluka, Buchs, Switzerland) in ultrapure water filtered through Milli-Q Gradient A10 filters (Millipore AG, Switzerland). The pH was adjusted to 7.4 using 6 M NaOH (Fluka, Buchs, Switzerland).

Polyelectrolytes and Polyelectrolyte Multilayers (PEM): Polyethylenimine (PEI, MW = 25 000 g/mol, branched, 408727), poly(allylamine hydrochloride) (PAH, MW = 70 000 g/mol, 283223), and poly(sodium 4-styrenesulfonate) (PSS, MW = 70 000 g/mol,

243051) were purchased from Sigma-Aldrich Chemie GmbH (Buchs, Switzerland). PEI, PAH, and PSS were dissolved at a concentration of 1 mg/mL in HEPES-2 buffer solution (150 mM NaCl). All of the solutions were sterile filtrated through 0.22 μm filters. PEM films were deposited with a custom-made automated spraying system. Four parallel Paasche VLS airbrushes (Paasche Airbrush Co., USA) connected to a compressor with pressure control allowed for the spraying of each polyelectrolyte or buffer solutions at a constant pressure (1 bar), with one airbrush for each different solution. A Lego Mindstorms NXT programmable robotics kit (Lego Group, Denmark) was used to fabricate a spraying device with programmable spraying time, pause time, and sequence order. The cleaned substrates were placed on a sample holder allowing for drainage of the solutions, fixed at a distance of 19 ± 2 cm from the airbrush aperture and tilted at 45°. Each solution was sprayed according to the following sequence: 5 s polyelectrolyte spraying, 15 s pause, 5 s buffer spraying, 5 s pause, so that the deposition of each bilayer required 1 min. For PSS/PAH films, the first layer of PAH was replaced by a PEI anchoring layer.

Lipids and Vesicle Preparation: 1,2-Dioleoyl-*sn*-glycero-3-phospho-L-serine (sodium salt) (DOPS, 840035) and 1-oleoyl-2-[12-[(7-nitro-2-1,3-benzoxadiazol-4-yl)amino]lauroyl]-*sn*-glycero-3-phosphocholine (NBD-PC, 810133) were purchased from Avanti Polar Lipids and stored in chloroform. Lipids (either pure DOPS or DOPS + 3% NBD-PC) were poured into a glass flask and completely dried with a nitrogen stream. Two 1 mL glass syringes were connected to a Teflon/steel extruder equipped with two 50 nm pore filters. Empty syringe 1 was mounted to the extruder, while HEPES-2 (1 mL, 150 mM NaCl) was added to the flask with the lipids (6 mg/mL), vortexed, and sucked into syringe 2. The solution was extruded 31 times. The vesicles were stored at 4 °C and used within a week.

Lipid Bilayer Formation: After the PEM deposition on the *trans* side, the chips were dried with a nitrogen gun and mounted in a vertical electrochemical cell similar to that described in ref 49. The buffer solution was preliminarily warmed up at 55 °C and poured in the electrochemical cell to hydrate the PEM. Dehydration and rehydration of PEM does not induce a serious change in the conformation of PEM as confirmed with AFM. Vesicle solution was also prewarmed up at 55 °C and simply added on the *cis* side of the chip for 20−30 min followed by a rinse.

Melittin: Melittin ($C_{131}H_{229}N_{39}O_{31}$) was purchased from Bio-Chemika (Fluka, Buchs, Switzerland). It is a cationic polypeptide composed of 26 amino acids (Gly-Ile-Gly-Ala-Val-Leu-Lys-Val-Leu-Thr-Thr-Gly-Leu-Pro-Ala-Leu-Ile-Ser-Trp-Ile-Lys-Arg-Lys-Arg-Gln-Gln-NH2) with a molecular weight of 2846.5 g/mol. It was stored at −20 °C in a freezer, and aliquots of 2−10 mg/mL were used to obtain the desired final concentration.

Atomic Force Microscopy (AFM): We used the Nanowizard I Bio-AFM (JPK Instruments, Berlin, Germany) and the Mikromasch CSC38/noAl cantilevers in contact mode (set point ∼1 nN, scan rate = 0.6−1.0 Hz).

Confocal Scanning Laser Microscope (CSLM) and Fluorescent Recovery after Photobleeching (FRAP): We used the LSM 510 microscope (Zeiss, Germany) equipped with an argon laser (488 nm) using a 40× (LD, NA 0.7) objective. The FRAP data were analyzed by evaluating intensity with ImageJ (Image processing and analysis in Java, National Institutes of Health; http://rsb.info.nih.gov). The diffusion coefficient was determined with the fitting procedure described in ref 43.

Electrochemical Impedance Spectroscopy (EIS): We used the Autolab PGSTAT12 Instrument (Ecochemie, Utrecht, The Netherlands), equipped with a FRA odule. Samples were positioned in a faraday cage. EIS spectra were recorded from 1 MHz to 0.01 Hz at 0 V offset potential applying 10 mV signal amplitude between two Ag/AgCl electrodes purchased from Lot-Oriel AG (WPI reference Electrode for EC-QCM Module QSP 020). The $I-V$ curve of Figure 4 was obtained with the same potentiostat using a sweep rate of 0.13 mV/s.

Supporting Information Available: Figure S1: detail of electrochemical impedance spectroscopy (EIS) analysis, Figure S2: single melittin channel events monitored after 1 and 2 weeks since the lipid bilayer was fabricated. This material is available free of charge *via* the Internet at http://pubs.acs.org.

REFERENCES AND NOTES

1. Mueller, P.; Rudin, D. O.; Ti Tien, H.; Wescott, W. C. Reconstitution of Cell Membrane Structure *In Vitro* and Its Transformation into an Excitable System. *Nature* **1962**, *194*, 979–980.
2. Ogier, S. D.; Bushby, R. J.; Cheng, Y.; Evans, S. D.; Evans, S. W.; Jenkins, A. T. A.; Knowles, P. F.; Miles, R. E. Suspended Planar Phospholipid Bilayers on Micromachined Supports. *Langmuir* **2000**, *16*, 5696–5701.
3. Bradley, R. J.; Urry, D. W.; Okamoto, K.; Rapaka, R. Channel Structures of Gramicidin—Characterization of Succinyl Derivatives. *Science* **1978**, *200*, 435–437.
4. Pawlak, M.; Stankowski, S.; Schwarz, G. Melittin Induced Voltage-Dependent Conductance in DOPC Lipid Bilayers. *Biochim. Biophys. Acta* **1991**, *1062*, 94–102.
5. Gomezlagunas, F.; Pena, A.; Lievano, A.; Darszon, A. Incorporation of Ionic Channels from Yeast Plasma-Membranes into Black Lipid-Membranes. *Biophys. J.* **1989**, *56*, 115–119.
6. Cornell, B. A.; BraachMaksvytis, V. L. B.; King, L. G.; Osman, P. D. J.; Raguse, B.; Wieczorek, L.; Pace, R. J. A Biosensor That Uses Ion-Channel Switches. *Nature* **1997**, *387*, 580–583.
7. Priscilla Kailian, A.; Kian Ping, L.; Thorsten, W.; Milos, N.; Emile Van, H. Supported Lipid Bilayer on Nanocrystalline Diamond: Dual Optical and Field-Effect Sensor for Membrane Disruption. *Adv. Funct. Mater.* **2009**, *19*, 109–116.
8. Yang, T.-H.; Yee, C. K.; Amweg, M. L.; Singh, S.; Kendall, E. L.; Dattelbaum, A. M.; Shreve, A. P.; Brinker, C. J.; Parikh, A. N. Optical Detection of Ion-Channel-Induced Proton Transport in Supported Phospholipid Bilayers. *Nano Lett.* **2007**, *7*, 2446–2451.
9. Zhou, X. J.; Moran-Mirabal, J. M.; Craighead, H. G.; McEuen, P. L. Supported Lipid Bilayer/Carbon Nanotube Hybrids. *Nat. Nanotechnol.* **2007**, *2*, 185–190.
10. Andersson, M.; Keizer, H. M.; Zhu, C.; Fine, D.; Dodabalapur, A.; Duran, R. S. Detection of Single Ion Channel Activity on a Chip Using Tethered Bilayer Membranes. *Langmuir* **2007**, *23*, 2924–2927.
11. Reimhult, E.; Zach, M.; Hook, F.; Kasemo, B. A Multitechnique Study of Liposome Adsorption on Au and Lipid Bilayer Formation on SiO₂. *Langmuir* **2006**, *22*, 3313–3319.
12. Schmitt, E. K.; Weichbrodt, C.; Steinem, C. Impedance Analysis of Gramicidin D in Pore-Suspending Membranes. *Soft Matter* **2009**, *5*, 3347–3353.
13. Han, X.; Studer, A.; Sehr, H.; Geissbühler, I.; Di Berardino, M.; Winkler, F. K.; Tiefenauer, L. X. Nanopore Arrays for Stable and Functional Free-Standing Lipid Bilayers. *Adv. Mater.* **2007**, *19*, 4466–4470.
14. Simon, A.; Girard-Egrot, A.; Sauter, F.; Pudda, C.; D'Hahan, N. P.; Blum, L.; Chatelain, F.; Fuchs, A. Formation and Stability of a Suspended Biomimetic Lipid Bilayer on Silicon Submicrometer-Sized Pores. *J. Colloid Interface Sci.* **2007**, *308*, 337–343.
15. Kresak, S.; Hianik, T.; Naumann, R. L. C. Giga-seal Solvent-Free Bilayer Lipid Membranes: From Single Nanopores to Nanopore Arrays. *Soft Matter* **2009**, *5*, 4021–4032.
16. Jeon, T. J.; Malmstadt, N.; Schmidt, J. J. Hydrogel-Encapsulated Lipid Membranes. *J. Am. Chem. Soc.* **2006**, *128*, 42–43.
17. Tanaka, M.; Sackmann, E. Polymer-Supported Membranes As Models of the Cell Surface. *Nature* **2005**, *437*, 656–663.
18. Wong, J. Y.; Majewski, J.; Seitz, M.; Park, C. K.; Israelachvili, J. N.; Smith, G. S. Polymer-Cushioned Bilayers. I. A Structural Study of Various Preparation Methods Using Neutron Reflectometry. *Biophys. J.* **1999**, *77*, 1445–1457.
19. Merzlyakov, M.; Li, E.; Gitsov, I.; Hristova, K. Surface-Supported Bilayers with Transmembrane Proteins: Role of the Polymer Cushion Revisited. *Langmuir* **2006**, *22*, 10145–10151.
20. Kohli, N.; Vaidya, S.; Ofoli, R. Y.; Worden, R. M.; Lee, I. Arrays of Lipid Bilayers and Liposomes on Patterned Polyelectrolyte Templates. *J. Colloid Interface Sci.* **2006**, *301*, 461–469.
21. Kang, X. f.; Cheley, S.; Rice-Ficht, A. C.; Bayley, H. A Storable Encapsulated Bilayer Chip Containing a Single Protein Nanopore. *J. Am. Chem. Soc.* **2007**, *129*, 4701–4705.
22. Shim, J. W.; Gu, L. Q. Stochastic Sensing on a Modular Chip Containing a Single-Ion Channel. *Anal. Chem.* **2007**, *79*, 2207–2213.
23. Decher, G. Fuzzy Nanoassemblies: Toward Layered Polymeric Multicomposites. *Science* **1997**, *277*, 1232–1237.

24. Sullivan, D. M.; Bruening, M. L. Ultrathin, Ion-Selective Polyimide Membranes Prepared from Layered Polyelectrolytes. *J. Am. Chem. Soc.* **2001**, *123*, 11805–11806.

25. Tang, Z.; Wang, Y.; Podsiadlo, P.; Kotov, N. A. Biomedical Applications of Layer-by-Layer Assembly: From Biomimetics to Tissue Engineering. *Adv. Mater.* **2006**, *18*, 3203–3224.

26. Xianghui, L.; Jingtao, Z.; David, M. L. Ultrathin Multilayered Films That Promote the Release of Two DNA Constructs with Separate and Distinct Release Profiles. *Adv. Mater.* **2008**, *20*, 4148–4153.

27. Tanaka, M.; Kaufmann, S.; Nissen, J.; Hochrein, M. Orientation Selective Immobilization of Human Erythrocyte Membranes on Ultrathin Cellulose Films. *Phys. Chem. Chem. Phys.* **2001**, *3*, 4091–4095.

28. Vockenroth, I. K.; Fine, D.; Dodobalapur, A.; Jenkins, A. T. A.; Köper, I. Tethered Bilayer Lipid Membranes with Giga-Ohm Resistances. *Electrochem. Commun.* **2008**, *10*, 323–328.

29. Moya, S.; Donath, E.; Sukhorukov, G. B.; Auch, M.; Baumler, H.; Lichtenfeld, H.; Mohwald, H. Lipid Coating on Polyelectrolyte Surface Modified Colloidal Particles and Polyelectrolyte Capsules. *Macromolecules* **2000**, *33*, 4538–4544.

30. Cassier, T.; Sinner, A.; Offenhäuser, A.; Möhwald, H. Homogeneity, Electrical Resistivity and Lateral Diffusion of Lipid Bilayers Coupled to Polyelectrolyte Multilayers. *Colloids Surf., B* **1999**, *15*, 215–225.

31. Volodkin, D.; Mohwald, H.; Voegel, J.-C.; Ball, V. Coating of Negatively Charged Liposomes by Polylysine: Drug Release Study. *J. Controlled Release* **2007**, *117*, 111–120.

32. Michel, A.; Izquierdo, A.; Decher, G.; Voegel, J. C.; Schaaf, P.; Ball, V. Layer by Layer Self-Assembled Polyelectrolyte Multilayers with Embedded Phospholipid Vesicles Obtained by Spraying: Integrity of the Vesicles. *Langmuir* **2005**, *21*, 7854–7859.

33. Schlenoff, J. B.; Dubas, S. T.; Farhat, T. Sprayed Polyelectrolyte Multilayers. *Langmuir* **2000**, *16*, 9968–9969.

34. Izquierdo, A.; Ono, S. S.; Voegel, J. C.; Schaaf, P.; Decher, G. Dipping *versus* Spraying: Exploring the Deposition Conditions for Speeding up Layer-by-Layer Assembly. *Langmuir* **2005**, *21*, 7558–7567.

35. Caruso, F.; Niikura, K.; Furlong, D. N.; Okahata, Y. Ultrathin Multilayer Polyelectrolyte Films on Gold: Construction and Thickness Determination. 1. *Langmuir* **1997**, *13*, 3422–3426.

36. Lavalle, P.; Gergely, C.; Cuisinier, F. J. G.; Decher, G.; Schaaf, P.; Voegel, J. C.; Picart, C. Comparison of the Structure of Polyelectrolyte Multilayer Films Exhibiting a Linear and an Exponential Growth Regime: An *In Situ* Atomic Force Microscopy Study. *Macromolecules* **2002**, *35*, 4458–4465.

37. Fischlechner, M.; Zaulig, M.; Meyer, S.; Estrela-Lopis, I.; Cuellar, L.; Irigoyen, J.; Pescador, P.; Brumen, M.; Messner, P.; Moya, S.; Donath, E. Lipid Layers on Polyelectrolyte Multilayer Supports. *Soft Matter* **2008**, *4*, 2245–2258.

38. Ai, S.; He, Q.; Tao, C.; Zheng, S.; Li, J. Conductive Polypyrrole and Poly(allylamine hydrochloride) Nanotubes Fabricated with Layer-by-Layer Assembly. *Macromol. Rapid Commun.* **2005**, *26*, 1965–1969.

39. Ai, S.; Lu, G.; He, Q.; Li, J. Highly Flexible Polyelectrolyte Nanotubes. *J. Am. Chem. Soc.* **2003**, *125*, 11140–11141.

40. Lee, D.; Nolte, A. J.; Kunz, A. L.; Rubner, M. F.; Cohen, R. E. pH-Induced Hysteretic Gating of Track-Etched Polycarbonate Membranes: Swelling/Deswelling Behavior of Polyelectrolyte Multilayers in Confined Geometry. *J. Am. Chem. Soc.* **2006**, *128*, 8521–8529.

41. Alem, H.; Blondeau, F.; Glinel, K.; Demoustier-Champagne, S.; Jonas, A. M. Layer-by-Layer Assembly of Polyelectrolytes in Nanopores. *Macromolecules* **2007**, *40*, 3366–3372.

42. Roy, C. J.; Dupont-Gillain, C.; Demoustier-Champagne, S.; Jonas, A. M.; Landoulsi, J. Growth Mechanism of Confined Polyelectrolyte Multilayers in Nanoporous Templates. *Langmuir* **2009**, *26*, 3350–3355.

43. Soumpasis, D. M. Theoretical Analysis of Fluorescence Photobleaching Recovery Experiments. *Biophys. J.* **1983**, *41*, 95–97.

44. Stanton, B. W.; Harris, J. J.; Miller, M. D.; Bruening, M. L. Ultrathin, Multilayered Polyelectrolyte Films as Nanofiltration Membranes. *Langmuir* **2003**, *19*, 7038–7042.

45. Lubke, L. L.; Garon, C. F. The Antimicrobial Agent Melittin Exhibits Powerful *In Vitro* Inhibitory Effects on the Lyme Disease Spirochete. *Clin. Infect. Dis.* **1997**, *25*, S48–S51.

46. Klotz, S. A.; Gaur, N. K.; Rauceo, J.; Lake, D. F.; Park, Y.; Hahm, K. S.; Lipke, P. N. Inhibition of Adherence and Killing of *Candida albicans* with a 23-Mer Peptide (Fn/23) with Dual Antifungal Properties. *Antimicrob. Agents Chemother.* **2004**, *48*, 4337–4341.

47. Lazarev, V. N.; Parfenova, T. M.; Gularyan, S. K.; Misyurina, O. Y.; Akopian, T. A.; Govorun, V. M. Induced Expression of Melittin, An Antimicrobial Peptide, Inhibits Infection by *Chlamydia trachomatis* and *Mycoplasma hominis* in a HeLa Cell Line. *Int. J. Antimicrob. Agents* **2002**, *19*, 133–137.

48. Raghuraman, H.; Chattopadhyay, A. Melittin: A Membrane-Active Peptide with Diverse Functions. *Biosci. Rep.* **2007**, *27*, 189–223.

49. Studer, A.; Han, X.; Winkler, F. K.; Tiefenauer, L. X. Formation of Individual Protein Channels in Lipid Bilayers Suspended in Nanopores. *Colloids Surf., B* **2009**, *73*, 325–331.

50. Tosteson, M. T.; Tosteson, D. C. The Sting. Melittin Forms Channels in Lipid Bilayers. *Biophys. J.* **1981**, *36*, 109–116.

51. Hanke, W.; Methfessel, C.; Wilmsen, H.-U.; Katz, E.; Jung, G.; Boheim, G. Melittin and a Chemically Modified Trichotoxin Form Alamethicin-Type Multi-State Pores. *Biochim. Biophys. Acta* **1983**, *727*, 108–114.

52. Stankowski, S.; Pawlak, M.; Kaisheva, E.; Robert, C. H.; Schwarz, G. A Combined Study of Aggregation, Membrane Affinity and Pore Activity of Natural and Modified Melittin. *Biochim. Biophys. Acta* **1991**, *1069*, 77–86.

53. Dubas, S. T.; Schlenoff, J. B. Swelling and Smoothing of Polyelectrolyte Multilayers by Salt. *Langmuir* **2001**, *17*, 7725–7727.

54. Steitz, R.; Jaeger, W.; von Klitzing, R. Influence of Charge Density and Ionic Strength on the Multilayer Formation of Strong Polyelectrolytes. *Langmuir* **2001**, *17*, 4471–4474.

55. Ladam, G.; Schaad, P.; Voegel, J. C.; Schaaf, P.; Decher, G.; Cuisinier, F. *In Situ* Determination of the Structural Properties of Initially Deposited Polyelectrolyte Multilayers. *Langmuir* **1999**, *16*, 1249–1255.

56. One may hypothesize the continuous increase of the current is because of the change in the thickness of the lipid bilayer due to the adsorption of melittin since recent works have revealed that adsorption of melittin onto the lipid bilayer stretches the bilayer and makes the bilayer thinner to induce a mechanical stress.[47] However, the hypothesis can be rejected because the thickness change by 60% is unreasonable compared to the reported change rate by 5% in PC systems.

57. Becucci, L.; Leon, R. R.; Moncelli, M. R.; Rovero, P.; Guidelli, R. Electrochemical Investigation of Melittin Reconstituted into a Mercury-Supported Lipid Bilayer. *Langmuir* **2006**, *22*, 6644–6650.

58. Hincha, D. K.; Crowe, J. H. The Lytic Activity of the Bee Venom Peptide Melittin Is Strongly Reduced by the Presence of Negatively Charged Phospholipids or Chloroplast Galactolipids in the Membranes of Phosphatidylcholine Large Unilamellar Vesicles. *Biochim. Biophys. Acta* **1996**, *1284*, 162–170.

59. Benachir, T.; Lafleur, M. Study of Vesicle Leakage Induced by Melittin. *Biochim. Biophys. Acta* **1995**, *1235*, 452–460.

60. Talbot, J. C.; Dufourcq, J.; de Bony, J.; Faucon, J. F.; Lussan, C. Conformational Change and Self Association of Monomeric Melittin. *FEBS Lett.* **1979**, *102*, 191–193.

61. Rex, S. Pore Formation Induced by the Peptide Melittin in Different Lipid Vesicle Membranes. *Biophys. Chem.* **1996**, *58*, 75–85.

62. Matsuzaki, K.; Yoneyama, S.; Miyajima, K. Pore Formation and Translocation of Melittin. *Biophys. J.* **1997**, *73*, 831–838.

63. Ladokhin, A. S.; Selsted, M. E.; White, S. H. Sizing Membrane Pores in Lipid Vesicles by Leakage of Co-encapsulated Markers: Pore Formation by Melittin. *Biophys. J.* **1997**, *72*, 1762–1766.

64. Lee, M.-T.; Hung, W.-C.; Chen, F.-Y.; Huang, H. W. Mechanism and Kinetics of Pore Formation in Membranes by Water-Soluble Amphipathic Peptides. *Proc. Natl. Acad. Sci. U.S.A.* **2008**, *105*, 5087–5092.

65. Heyderman, L. J.; Ketterer, B.; Bachle, D.; Glaus, F.; Haas, B.; Schift, H.; Vogelsang, K.; Gobrecht, J.; Tiefenauer, L.; Dubochet, O.; Surbled, P.; Hessler, T. High Volume Fabrication of Customised Nanopore Membrane Chips. *Microelectron. Eng.* **2003**, *67*—*8*, 208–213.